Eur. Phys. J. D **31**, 469–475 (2004)
DOI: 10.1140/epjd/e2004-00180-5

THE EUROPEAN PHYSICAL JOURNAL D

Abstraction and insertion mechanisms in reactive collisions of H_2^+ and D_2^+ with O^-

E.M. Staicu-Casagrande[1,a], T. Nzeyimana[1], E.A. Naji[1], N. de Ruette[1], B. Fabre[1], A. Le Padellec[2], and X. Urbain[1,b]

[1] Unité FYAM, Département de Physique, Université Catholique de Louvain, Chemin du cyclotron 2, 1348 Louvain-La-Neuve, Belgium
[2] LCAR UMR 5589, Université Paul Sabatier-Toulouse III, 118 route de Narbonne, bâtiment IIIR1b4, 31062 Toulouse Cedex 4, France

Received 31 March 2004 / Received in final form 4 October 2004
Published online 6 December 2004 –

Abstract. Integral cross-sections were measured for the associative ionisation and reactive ionisation in collisions of H_2^+ and D_2^+ with O^- by means of a merged-beam set-up operating with keV beams. The magnitude of the reactive cross-sections is quite large (10^{-14} cm^2 at 10 meV), and surpasses the associative ionisation by an order of magnitude. The observed ratio is discussed in terms of insertion and abstraction mechanisms that prevail in the case of atom-diatom inelastic collisions. These measurements may be relevant to the understanding of some astrophysical objects such as the comets, where the presence of the water cation was highlighted.

PACS. 82.30.Nr Association, addition, insertion, cluster formation – 31.10.+z Theory of electronic structure, electronic transitions, and chemical binding – 95.30.Ft Molecular and chemical processes and interactions

1 Introduction

The water molecule, due to its key role in various branches of science, was intensely studied and documented. Not only its properties as an isolated molecule are crucial to characterize and to understand, but also its formation and destruction pathways. Whereas the destruction of H_2O was extensively investigated, for collisions with partners such as photons [1], atoms [2] and molecules [3], the formation of H_2O has received less attention up to now. There are two main ways to form water molecules: from elementary reactants such as H, H_2, OH and O, or from the fragmentation of more complex water-containing systems, such as H_3O^+. When built from elementary blocks, the energy brought into the associated system is non-negligible, and consequently it would need to relax with in turn, an overwhelmingly large dissociation probability. Most of the theoretical effort so far dealt with the reactive scattering of H_2 molecules with O(^{3}P, ^{1}D), that are relevant to the formation of the OH radical [4–7]. For the O(^{3}P) reactant, the nature and role of the quantized transition states of H_2O were carefully studied theoretically and reported by Chatfield et al. [8]. The structures they observed could be assigned to stretch-bend-rotation states of the activated transition states which, in turn, break into OH + H. Several investigations dealing with the reaction of the same diatom but with the metastable O(^{1}D) atom were carried out, indeed a much more efficient channel than that arising from the triplet state, due to its exothermicity and the absence of reaction barrier along the reaction path [4].

Whereas water had been seen in the interstellar medium for decades [9], its charged counterpart H_2O^+ was discovered much more recently, in the Comet 1995 O1 Hale-Bopp [10]. This ion is not only quite well understood from the point of view of its spectroscopy (at least for the three lowest states) [11,12], but also from several dynamical aspects connected to collisions with photons (in the nanosecond and femtosecond regimes) [13], as well as with electrons [14]. Concerning these latter projectiles, several recent studies were carried out on the dissociative recombination process, indeed an important destruction mechanism of the water cation [15,16]. A recent and important breakthrough came from an imaging study of the three-body fragmentation dynamics via dissociative recombination, coupled with theoretical modelling calculations [16]. The two-body break-up, although not studied with such level of refinement, was quantified and for instance, (9 ± 4)% of the dissociative flux was found

[a] *Present address*: Laboratoire des Collisions Atomiques et Moléculaires, Université Paris XI, 91405 Orsay Cedex, France.
[b] e-mail: urbain@fyam.ucl.ac.be

to flow to the O + H_2 channel [15]. To the best of our knowledge, the reverse process, that of associative ionisation (AI) from neutral products, was never studied, nor reported. The very same process, but from the charged species H_2^+ (or D_2^+) + O^-, was not studied either, until the work presented here. Similarly, the dissociative excitation of H_2O^+ and HDO^+ by electron impact was studied by Jensen et al. [14], and branching ratios for the production of H, OH and O fragments were determined. The reverse process is not easily observed, since it would involve a three-body collision. Instead, the reactive scattering of H_2^+ and D_2^+ with O atoms was investigated by McClure et al. [17] using a merged beam apparatus. The same reactive channel, i.e. the production of the OH^+ and OD^+ radicals, is also part of the present work dealing with H_2^+ + O^- and D_2^+ + O^- collisions.

The paper is organized as follows. The next section will briefly present the experimental set-up and procedure, the list of observable reactions and the degree of internal excitation of the reactants and products. This is followed by the presentation and detailed discussion of our data, in terms of energy dependence, absolute magnitude and possible reaction mechanisms. A conclusion is finally given.

2 Experiment

A detailed description of the merged beam apparatus of Louvain-la-Neuve can be found elsewhere [18]. In brief, the whole set-up is divided into four sections (Fig. 1): a first one that includes two ion sources with their respective mass selectors and beam optics, a second one where the two ion beams are merged, a third one that corresponds to the interaction region, and a last one that contains a magnetic analyser, Faraday cups and the particle detector. The interaction region is defined by an observation voltage applied on a set of electrodes coaxial with the beam. The energy of the molecular ions is analysed in a magnetic spectrograph to select those produced inside the biased region, and their number is counted on a large channel electron multiplier behind a cylindrical electrostatic deflector that screens the detector against scattered particles and UV photons.

The number of reaction events N, which occur during the acquisition time T, is related to the absolute cross-section σ in a merged beam set-up, by:

$$N(T) = \sigma \frac{v_r}{q_1 q_2 v_1 v_2} F \int_0^T I_1(t) I_2(t) dt. \qquad (1)$$

The relative velocity, the laboratory velocities of the two beams, their charges ($\pm e$) and intensities, are depicted by v_r, v_1, v_2, q_1, q_2, I_1 and I_2, respectively. The time independent form factor F accounts for the degree of overlap of the interacting beams.

In practice, the two beams are strongly collimated just before they interact, and one makes use only of the cores

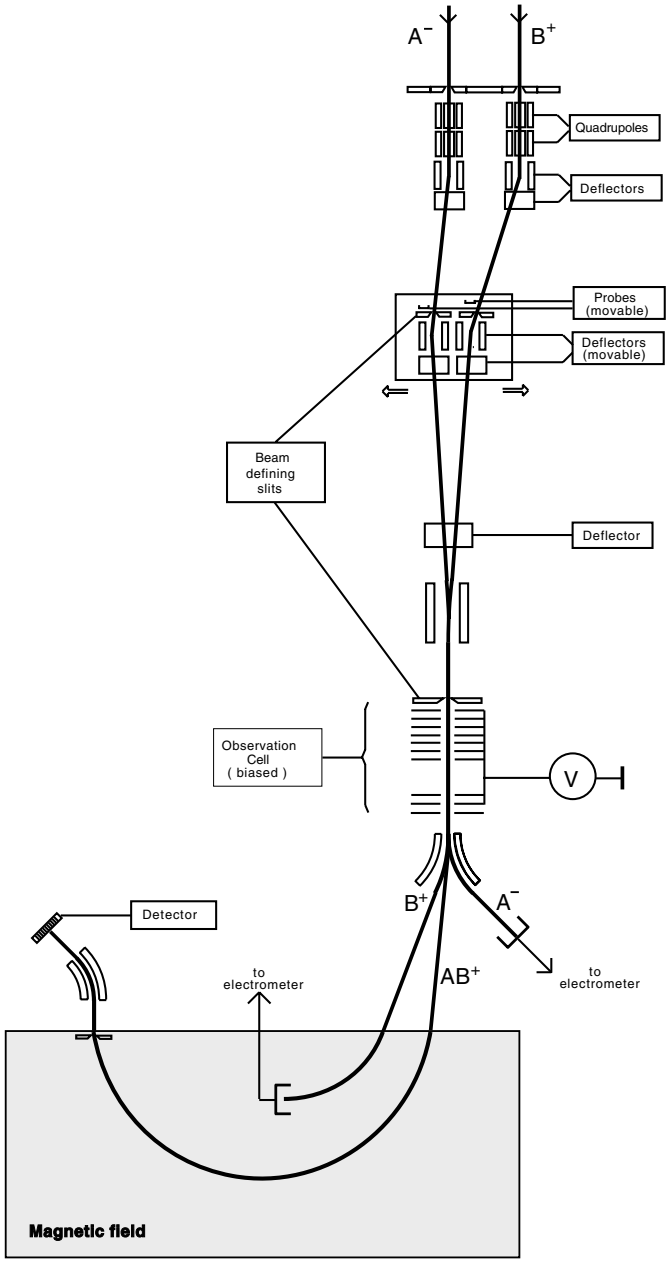

Fig. 1. Sketch of the merged beam apparatus. Optical elements and ion trajectories are not to scale.

of the two reactant beams. The background contribution, though seriously reduced with the addition of a cylindrical deflector, had to be evaluated for the same acquisition time T by chopping the anionic beam, and subtracted from the apparent signal. The issue connected to the energy resolution was detailed elsewhere [18] and is therefore not repeated here. The relative velocity distribution at equal mean velocities of the two beams produces a nearly Maxwellian distribution at an equivalent temperature of 100 K.

The O^- beam was extracted off-axis from a duoplasmatron ion source filled with pure N_2O, and accelerated to

13 keV. There is no possible internal excitation of the O^- beam, since only the ground state $2p^5\ ^2P_{3/2}$ is stable. An ECR ion source, placed 2.6 m upstream from the interaction region, produced the H_2^+ and D_2^+ beams from pure hydrogen and deuterium, respectively. The ions were accelerated to energies ranging between 2.5 and 4 keV, depending on the mass ratio of the reactants and the observation voltage applied. Von Busch and Dunn [19] performed a photodissociation study of H_2^+ and D_2^+ in the $^2\Sigma_g^+$ $(1s\sigma_g)$ ground state and measured the vibrational populations up to the dissociation limit, i.e. $v = 18$ for H_2^+. They showed that H_2^+, when produced by electron impact, is significantly vibrationally excited, the five first levels being populated by more than 10% each. These can not decay before reaching the interaction region since vibration-rotation transitions of homonuclear molecules are forbidden in the electric dipole approximation. The quadrupole terms give lifetimes of the order of 10^6 s, for v up to 10 [20].

Although the principle of operation of an ECR source lies in the direct heating of electrons in their cyclotron motion, one may expect some heat transfer to the ions to occur in the plasma created by the microwave power fed into the source. In order to quantify this assumption, we have connected our kinetic energy release spectrometer [21,22] to the present apparatus. The measurement relies on the population, through charge exchange with an alkali target, of a long-lived Rydberg state of the H_2/D_2 molecule. The $c^3\Pi_u$ state is rotationally predissociated by the $b^3\Sigma_u^+$ state and decays into a pair of H/D atoms, within a few nanoseconds for the lowest rovibrational state, and picoseconds for the higher lying states. The spectrometer itself consists of an effusive potassium target, followed by a two-meter long drift tube equipped with a pair of position-sensitive detectors operating in coincidence. From the position and relative time of arrival of each fragment, energy and momentum conservation allows the determination of the kinetic energy released in the centre-of-mass frame, with a resolution of 100 meV in the range of interest, i.e. 7 to 10 eV. De Bruijn and Los [23] have demonstrated the close correspondence of the area of the predissociation peaks appearing in the kinetic energy release spectrum with the populations determined by von Busch and Dunn [19] by fitting their photodissociation spectra over a broad wavelength range. Our measurements for H_2^+ and D_2^+ produced under standard conditions by the ECR source and accelerated to 7 keV are plotted in Figures 2a and 2b respectively, together with the calculated distribution for electron impact ionisation. A marked difference is seen for H_2^+, and some for D_2^+, mostly in the population of high-lying vibrational levels. To account for this discrepancy, one has to assume some population of the $v \geq 1$ levels of H_2 and D_2, as it may arise from charge exchange between ions and neutral molecules. However, as the source operates at quite low pressure ($<5 \times 10^{-4}$ mbar), the ions are not expected to contribute significantly to heating. On the other hand, the anharmonicity of the H_2 potential well favours energy pooling transitions between excited molecules, populating vibrational levels far above k_BT.

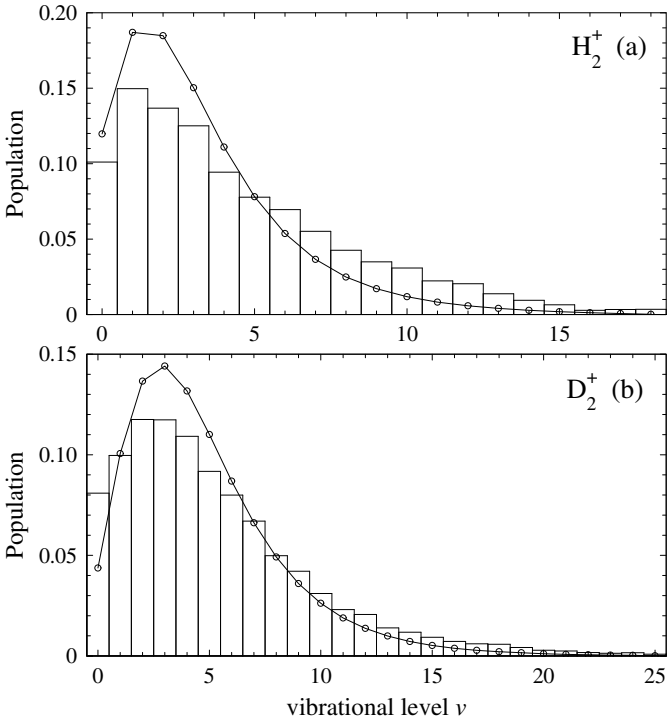

Fig. 2. Vibrational populations (bars) measured by dissociative charge exchange of H_2^+ (a) and D_2^+ (b) on a potassium target. Connected symbols represent the population produced by electron impact ionisation of ground state H_2/D_2, as modelled by von Busch and Dunn [19].

In the collisions of H_2^+ (D_2^+) with O^-, numerous channels are open at low energy :

$$H_2^+(X^2\Sigma_g^+) + O^-(^2P)$$
$$\rightarrow H_2O(\tilde{X}^1A_1) + h\nu(19.2\text{ eV}) \quad (2a)$$
$$\rightarrow H_2(X^1\Sigma_g^+) + O(^3P) + 14.2\text{ eV} \quad (2b)$$
$$\rightarrow OH(X^2\Pi) + H + 14.1\text{ eV} \quad (2c)$$
$$\rightarrow H + H + O(^3P) + 9.4\text{ eV} \quad (2d)$$
$$\rightarrow H_2O^+(\tilde{X}^2B_1) + e + 6.6\text{ eV} \quad (2e)$$
$$\rightarrow OH^-(X^1\Sigma^+) + H^+ + 2.3\text{ eV} \quad (2f)$$
$$\rightarrow OH^+(X^3\Sigma^-) + H^- + 1.9\text{ eV} \quad (2g)$$
$$\rightarrow OH^+(X^3\Sigma^-) + H + e + 1.1\text{ eV} \quad (2h)$$
$$\rightarrow OH(X^2\Pi) + H^+ + e + 0.5\text{ eV} \quad (2i)$$
$$\rightarrow H_2(X^1\Sigma_g^+) + O^+(^4S) + e + 0.3\text{ eV}. \quad (2j)$$

Our experimental set-up allows the detection of heavy positive products, such as H_2O^+ (D_2O^+) and OH^+ (OD^+), corresponding to processes (2e) and (2g)+(2h) respectively. Reactions (2e) and (2h) are the result of the same autoionisation process, leading in the first case to the formation of the molecular cation (associative ionisation, AI) in competition with its dissociated form, $OH^+ + H$ in the latter case (hereafter referenced to as reactive ionisation, RI).

In monitoring the production of OH^+ and H_2O^+ ions, we are only sensitive to their mass, but not their internal state. At 0 eV, three electronic states of H_2O^+ may be populated: $\tilde{X}^2B_1$ (equilibrium geometry close to the neutral ground state, $\theta_{OH} = 110.46°$, $R_{OH} = 0.999$Å), $\tilde{A}^2A_1$ (linear, $R_{OH} = 0.981$Å) and $\tilde{B}^2B_2$ ($\theta_{OH} = 54.98°$, $R_{OH} = 1.140$Å) [24–26]. The $\tilde{X}^2B_1 \leftarrow \tilde{A}^2A_1$ emission spectrum was detected and the lifetimes of the levels were reported at (10.5±1) μs [27]. These are comparable to the 4.1 μs time of flight of the H_2O^+ ions between the interaction region and the channeltron detector. No fluorescence was ever reported from the $\tilde{B}^2B_2$ state, and consequently this intriguing nonradiative decay was the subject of several investigations. A paper by Reutt et al. [13] put forward a possible mechanism for the decay, based on a diabatic surface crossing (conical intersection) between the $\tilde{B}^2B_2$ and $\tilde{A}^2A_1$ states, near the minimum of the former one. It was demonstrated that a wave packet, prepared on the $\tilde{B}^2B_2$ surface and travelling along the ν_2 coordinate (bending mode), can pass through the seam of the intersection and can hop onto the $\tilde{A}^2A_1$ surface, all that on a 10^{-14} s time scale. Clearly, our measurements refer to mixtures of $\tilde{A}^2A_1$ and $\tilde{X}^2B_1$ states (ro-vibrationally excited) that do not necessarily reflect the production patterns in the interaction region. Moreover, while increasing the relative energy, higher electronic states of the H_2O^+ ion become accessible (not much documented in the literature), and among them, the lowest $\tilde{a}^4B_1$ state [28] (relative energies larger than 6.9 eV).

Regarding OH^+ and OD^+ products, these may only be formed in their electronic ground state $X\,^3\Sigma^-$. At increasing collision energies though, additional channels become accessible, among which the $A\,^3\Pi$ state. The radiative lifetime of its ground vibrational level has been measured by Brzozowski et al. [29] and found to be 0.89 μs for OH^+, 1.06 μs for OD^+. This is substantially shorter than the time of flight of the ions to the detector. Other excited states like the $a\,^1\Delta$ and $b\,^1\Sigma^+$ are known to be spin-orbit coupled to the aforementioned triplet states [30].

3 Results and discussion

The absolute AI and RI cross-sections measured for reactions (2e) and (2g)+(2h) respectively are shown in Figure 3 for $H_2^+ + O^-$ and $D_2^+ + O^-$ collisions as a function of relative energy, up to 20 eV. The energy resolution of the apparatus is such that we restricted our presentation to energies greater than 5 meV (see Ref. [18]). The error bars along the vertical axis represent only the statistical uncertainties; 6% systematic uncertainties should be added. Clearly, the reactive processes (reactions (2g) and (2h)) dominate the ionisation of the system, being one order of magnitude above AI. Furthermore, a slight enhancement of the RI process is present when substituting D_2^+ for H_2^+, while no such difference is visible in the AI channel. The monotonous decrease of all cross-sections observed at low energy is typical of a pure Coulomb interaction (see discussion in [18]). The full line was obtained by

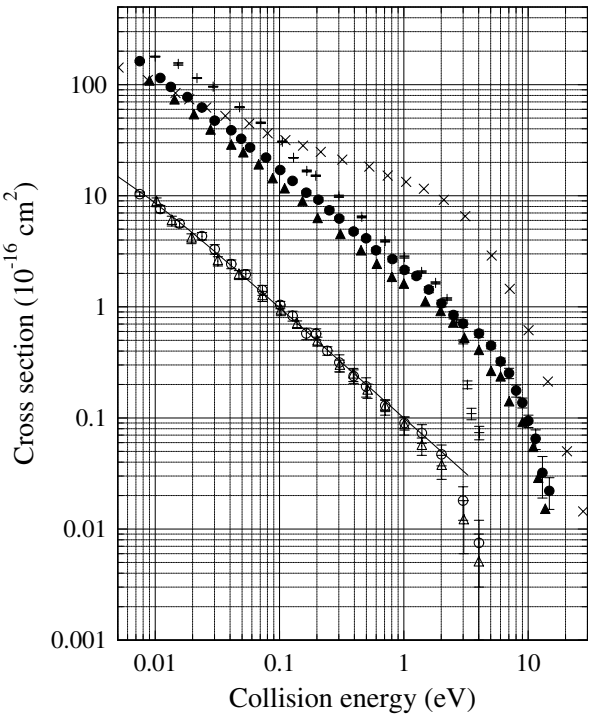

Fig. 3. Integral AI (open marks) and RI (full marks) cross-sections as a function of relative energy: triangles — $H_2^+ + O^-$ collisions; circles — $D_2^+ + O^-$ collisions; plus signs — AI in $D^+ + O^-$ collisions [32]; crosses — reactive scattering in $D_2^+ + O$ collisions [17]; full line — E^{-1} model cross-section folded with the experimental relative energy distribution.

folding the calculated collision energy distribution with a model cross-section having a E^{-1} energy dependence, and appears to fit the data remarkably well. We recall that, for a diatomic system, the low energy AI cross-section can be written as [31]:

$$\sigma = \pi \frac{R_e^2 DP}{E} \tag{3}$$

where the parameter R_e depicts the equilibrium distance of the associated system, D its binding energy and P the combined probability for populating a reactive potential energy surface and undergoing autoionisation along it. The simple reasoning represented by equation (3), relates in fact the impact parameter with the binding energy corresponding to a specific vibrational state (a unique mode) of the associated system. For polyatomic systems, several vibrational modes have to be considered, and each of them is differently affected by the centrifugal potential associated with the relative motion of the reactants. This may slightly influence the overall exponent in formula (3).

Figure 4 displays the thermal rate coefficients for associative ionisation and reactive ionisation in $H_2^+ + O^-$ and $D_2^+ + O^-$ collisions (in cm^3s^{-1}) as a function of the ionic temperature (in K). These coefficients, useful for plasma (natural or laboratory-made) studies, are derived from the following relation

$$\alpha(T) = \frac{8\pi\mu}{(2\pi\mu k_B T)^{3/2}} \int_0^\infty \sigma(E) E e^{-E/k_B T} dE \tag{4}$$

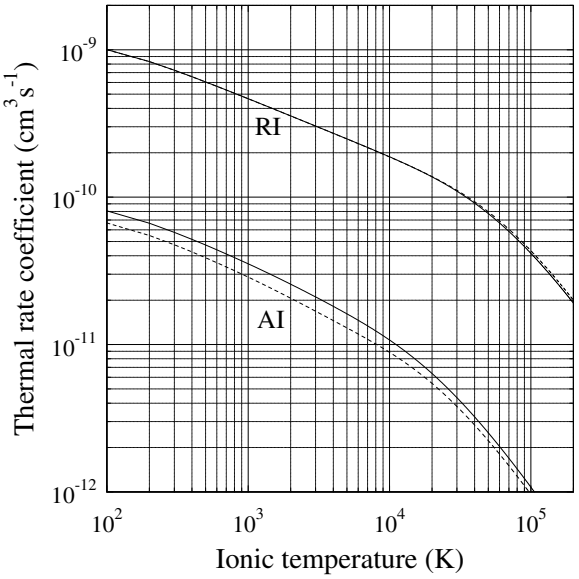

Fig. 4. AI and RI thermal rate coefficients versus ionic temperature: full lines — $H_2^+ + O^-$ collisions; dashed lines — $D_2^+ + O^-$ collisions.

where μ is the reduced mass of the system and σ is the experimental cross-section. These rate coefficients are particularly relevant when the ionic temperature is lower than 17000 K, the equivalent to the 1.46 eV electron affinity of the oxygen atom. The perfect overlap of the RI reaction rates happens as a result of the aforementioned isotope effect, that makes the measured cross-sections approximately scale with $\sqrt{\mu}$.

Also plotted in Figure 3 (crosses) is the cross-section measured by McClure et al. [17] for reaction

$$D_2^+(X^2\Sigma_g^+) + O(^3P) \rightarrow OD^+(X^3\Sigma^-) + D \qquad (5)$$

with a similar apparatus. This atom-molecular ion reaction occurs on a single potential energy surface, and exhibits the expected Langevin behaviour, its cross-section varying as $1/v$. The present results for the RI process exceed that of direct reactive scattering below 0.02 eV, as a result of the larger capture range of the Coulomb potential, while they become one order of magnitude lower at 1 eV, due to their E^{-1} dependence. This strong departure stems from the limited range of the molecular autoionisation, which in turn limits the efficiency of the AI and RI processes at higher energy.

The absolute magnitude of the AI and RI cross-sections may further be compared to those measured earlier for AI in the $D^+ + O^-$ isobaric system [32], as plotted in Figure 3 (plus signs). While the $D^+ + O^-$ and $H_2^+ + O^-$ collisional systems obviously differ by the type of chemical bond to be formed, they exhibit similar binding energies and equilibrium distances, which are relevant parameters for the access to the autoionisation continuum after mutual attraction along the Coulombic potential at equal relative velocities. The total cross-section measured for $D^+ + O^-$ is about 3 times larger than the sum of AI and RI cross-sections in the $H_2^+ + O^-$ case. This large ratio may be explained by the missing contribution of the (2f) and (2i) channels. Both reactions produce H^+, that can not be detected in the present experiment, since they are buried in the huge background of collisional dissociation of H_2^+. A tentative comparison with the branching ratios measured by Jensen et al. [14] for the dissociative excitation of H_2O^+ by electron impact indicates that $OH^+ + H$ and $OH + H^+$ channels are equally important at threshold, i.e. the cross-sections for processes (2h) and (2i) are of similar magnitude, accounting for most of the difference between the diatomic and triatomic cases.

The magnitude of the AI cross-section itself may be quite surprising when compared to the $D^+ + O^-$ case. A first difference between the two systems lies in the relative position of the dissociation thresholds of the molecular complex. In the present case, the dissociation limit of H_2O^+ lies 1.1 eV below the entrance channel, while it lies 1.46 eV above in the $D^+ + O^-$ case. The dissociation continuum is thus accessible right from threshold, explaining both the large cross-section of the RI process and the small cross-section for AI.

A second difference lies in the increased complexity of the triatomic system. Even if the various reaction channels certainly display cross-sections of various amplitudes, some must be large such as the long range mutual neutralisation process (for which no data are available in the literature) or the five shorter range abstraction channels that do not prevail in the diatomic case. The flux that goes to the associative ionisation channel, the result of an insertion mechanism, is therefore somewhat limited (counterbalanced) by the various abstraction channels (2c), (2f–2i). Indeed, with such a light and rotating H_2^+ target, the probability for the O^- projectile to approach along the median of the H_2-axis is small whereas that of colliding with one of the two hydrogen atoms is large. However, such a dichotomy between abstraction and insertion processes may be questionable for strongly attractive potential energy surfaces like those involved in the collision of a positive with a negative ion, as discussed below.

According to the mechanisms described by Buss et al. [33], OH production (reactions (2c), (2f–2i)) can result either from the abstraction of a proton or from the insertion of the oxygen atom, while H_2O^+ may only result from the insertion of the O atom to the centre of the H_2 bond. In terms of collision geometries, abstraction is efficient in the collinear approach of the reactants, where direct rebound on the potential barrier leads to proton transfer, with substantial vibrational excitation. On the other hand, the insertion is typical of an attractive surface of the complex, and leads to rotationally excited products, as demonstrated by Aoiz et al. [6].

The RI channel, with formation of OH or OH^+, further differs from AI by the fact that the transition state may decay by autoionisation to repulsive states or bound states that are predissociated. The latter are typical of an insertion reaction, while the former lead to rebound dynamics and abstraction. It is generally believed for the neutral case that the reactive scattering mainly proceeds through the insertion of O atom into H_2 to produce

highly excited H_2O intermediate which is probably short-lived [4]. The efficient OH^+ formation is in agreement with the H_2O^+ dissociative excitation experiments of Jensen et al. [14],where the H and OH channels dominate, indicating that the dissociation process preferentially breaks a single OH bond. In our case we believe that the extensive rotational excitation characterizing all heavy-particle collisions triggers the dissociation of the molecular system.

Whereas the Coulomb potential tends to randomize the orientation of the H_2^+ molecule with respect to the reaction coordinate, increasing collision energies may favour the collinear approach. Indeed, in their study of OD^+ formation in $D_2^+ + O$ collisions [17], McClure et al. concluded that the rebound dynamics and hence the abstraction mechanism were dominating at energies above a few eV, as demonstrated by the strong forward scattering of the OD^+ products. An analysis of the vibrational and rotational excitation of the OH^+ (OD^+) products would certainly help in this matter.

Finally, the more efficient production of OD^+ than OH^+ by a factor 1.4, close to the ratio of reduced masses, i.e. the inverse of the ratio of relative velocities at a given collision energy, points to a characteristic time for autoionisation and/or rearrangement as a key parameter for the efficiency of the RI process.

We shall now dwell on the high energy part of Figure 3. Among the various channels that are energetically open over the energy range 0–15 eV,

$$
\begin{aligned}
&H_2^+(X^2\Sigma_g^+) + O^-(^2P) \\
&\quad \rightarrow H_2^+(X^2\Sigma_g^+) + O(^3P) + e - 1.5 \text{ eV} && \text{(6a)}\\
&\quad \rightarrow H^+ + H + O^-(^2P) - 2.7 \text{ eV} && \text{(6b)}\\
&\quad \rightarrow H^+ + H^- + O(^3P) - 3.5 \text{ eV} && \text{(6c)}\\
&\quad \rightarrow H^- + H + O^+(^4S) - 3.5 \text{ eV} && \text{(6d)}\\
&\quad \rightarrow H^+ + H + O(^3P) + e - 4.2 \text{ eV} && \text{(6e)}\\
&\quad \rightarrow H + H + O^+(^4S) + e - 4.2 \text{ eV} && \text{(6f)}\\
&\quad \rightarrow OH^+(X^3\Sigma^-) + H^+ + 2e - 12.5 \text{ eV} && \text{(6g)}
\end{aligned}
$$

three of them require the least rearrangement: the detachment of the O^- projectile (6a), the dissociation of the H_2^+ target (6b) and the dissociative detachment (6e). It is tempting to attribute the sudden drop of the RI cross-sections above 4 eV to channel (6e), as it corresponds to the dissociation limit of the OH^+ product. Channels (6a) and (6b) do not seem to affect the RI channel, while the AI cross-sections fall more rapidly above the detachment threshold, as observed in a previous study of $C^+ + O^-$ collisions [18].

Describing and rationalizing every feature that appears in the spectrum is however a difficult task, due to the degree of excitation of the H_2^+ and D_2^+ reactants (rotation and vibration). According to the present measurements, only 60% of the vibrational population of H_2^+ lies between $v = 0$ and $v = 5$. The consequence is that every threshold would have to be lowered by 0.97 eV on average, provided the products are in their ground state, which is rather doubtful, as discussed at the end of the preceding section. The internal excitation measured for H_2^+ and D_2^+ does influence the energetics of the reactions, but to a limited extent. Indeed, the threshold for reaction (6a) is not expected to be lowered, as the H_2^+/D_2^+ reactant remains essentially unaffected by the collision. On the other hand, reaction (6b) is increasingly likely as one goes up with vibrational excitation. However, this discussion does not apply to rotational excitation, possibly important in the present case but difficult to quantify.

4 Conclusion

Cross-sections for the associative ionisation and reactive ionisation processes in $H_2^+ + O^-$ and $D_2^+ + O^-$ collisions were measured using our merged beam set-up. Special attention was drawn to the internal energy of the target H_2^+ (D_2^+) ions, which were fully characterized for the first time in such measurements. Our main result concerns the relatively large size of the measured RI cross-sections, indicating the propensity of the transition complex to break an OH (OD) bond, by fast rebound dynamics typical of abstraction processes. On the other hand, the small AI cross-section may be accounted for by the necessary insertion of the O atom in the middle of the H_2 (D_2) molecule, a much less favorable process as far as the collision geometry and the rotational excitation of the complex are considered.

This work was funded by the Belgian National Fund for Scientific Research (FNRS) and the Euratom-Belgian state association. EMSC was a postdoctoral fellow of the IHP program of EC under contract HPRN-CT-2000-00142. XU is a Research Associate of the FNRS.

References

1. D.H. Mordaunt, M.N.R. Ashfold, R.N. Dixon, J. Chem. Phys. **100**, 7360 (1994)
2. X. Li, Y.-L. Huang, G.D. Flesch, C.Y. Ng, J. Chem. Phys. **106**, 928 (1997)
3. S. Gardner, R.A. Dressler, R.H. Salter, E. Murad, J. Chem. Phys. **97**, 2473 (1992)
4. T. Peng, D.H. Zhang, J.Z.H. Zhang, R. Schinke, Chem. Phys. Lett. **248**, 37 (1996)
5. M. Alagia, N. Balucani, L. Cartechini, P. Casavecchia, E.H. van Kleef, G.G. Volpi, P.J. Kuntz, J.J. Sloan, J. Chem. Phys. **108**, 6698 (1998)
6. F.J. Aoiz, L. Banares, J.F. Castillo, V.J. Herrero, B. Martinez-Haya, P. Honvault, J.M. Launay, X. Liu, J.J. Lin, S.A. Harich, C.C. Wang, X. Yang, J. Chem. Phys. **116**, 10692 (2002)
7. N. Balakrishnan, J. Chem. Phys. **119**, 195 (2003)
8. D.C. Chatfield, R.S. Friedman, G.C. Lynch, D.G. Truhlar, D.W. Schwenke, J. Chem. Phys. **98**, 342 (1993)
9. A.C. Cheung, D.M. Rank, C.H. Townes, D.D. Thornton, W.J. Welch, Nature **221**, 626 (1969)

10. D.G. Kupperman, L.J. Paxton, J. Carbary, G.J. Romick, D.E. Anderson, C.-I. Meng, P.D. Feldman, Geophys. Res. Lett. **25**, 3261 (1998)
11. J.C. Leclerc, J.A. Horsley, J.C. Lorquet, Chem. Phys. **4**, 337 (1974)
12. A.J. Lorquet, J.C. Lorquet, Chem. Phys. **4**, 353 (1974)
13. J.E. Reutt, L.S. Wang, Y.T. Lee, D.A. Shirley, J. Chem. Phys. **85**, 6928 (1986)
14. M.J. Jensen, R.C. Bilodeau, O. Heber, H.B. Pedersen, C.P. Safvan, X. Urbain, D. Zajfman, L.H. Andersen, Phys. Rev. A **60**, 2970 (1999)
15. S. Rosen, A. Derkatch, J. Semaniak, A. Neau, A. Al-Khalili, A. Le Padellec, L. Vikor, R. Thomas, H. Danared, M. af Ugglas, M. Larsson, Faraday Discuss. **115**, 295 (2000)
16. R. Thomas, S. Rosen, F. Hellberg, A. Derkatch, M. Larsson, S. Datz, R. Dixon, W.J. van der Zande, Phys. Rev. A **66**, 032715 (2002)
17. D.J. McClure, C.H. Douglass, W.R. Gentry, J. Chem. Phys. **67**, 2362 (1977)
18. T. Nzeyimana, E.A. Naji, X. Urbain, A. Le Padellec, Eur. Phys. J. D **19**, 315 (2002)
19. F. von Busch, G.H. Dunn, Phys. Rev. A **5**, 1726 (1972)
20. J.M. Peek, A.-R. Hashemi-Attar, C.L. Beckel, J. Chem. Phys. **71**, 5382 (1979)
21. V.M. Andrianarijaona, Ph.D. thesis, Université catholique de Louvain, 2002 (unpublished)
22. X. Urbain, B. Fabre, E.M. Staicu-Casagrande, N. de Ruette, V.M. Andrianarijaona, J. Jureta, J.H. Posthumus, Phys. Rev. Lett. **92**, 163004 (2004)
23. D.P.de Bruijn, J. Los, Rev. Sci. Instrum. **53**, 1020 (1982)
24. H. Lew, Can. J. Phys. **54**, 2028 (1976)
25. P.C. Hariharan, J.A. Pople, Mol. Phys. **27**, 209 (1974)
26. P.J. Fortune, B.J. Rosenberg, A.C. Wahl, J. Chem. Phys. **65**, 2201 (1976)
27. G.R. Mohlmann, K.K. Bhutani, F.J. DeHeer, S. Tsurubuchi, Chem. Phys. **31**, 273 (1978)
28. H.H. Harris, J.J. Leventhal, J. Chem. Phys. **64**, 3185 (1976)
29. J. Brzozowski, N. Elander, P. Erman, M. Lyyra, Phys. Scripta **10**, 241 (1974); J. Brzozowski, P. Erman, H. Lew, Chem. Phys. Lett. **34**, 267 (1975)
30. A.J. Merer, D.N. Malm, R.W. Martin, M. Horani, J. Rostas, Can. J. Phys. **53**, 251 (1975)
31. F. Brouillard, X. Urbain, Phys. Scripta **96**, 86 (2002)
32. E.A. Naji, T. Nzeyimana, X. Urbain, A. Le Padellec, J. Phys. B **35**, 4325 (2002)
33. R.J. Buss, P. Casavecchia, T. Hirooka, S.J. Sibener, Y.T. Lee, Chem. Phys. Lett. **82**, 386 (1981)